The photochemical ring-opening of 1,3-cyclohexadiene imaged by ultrafast electron diffraction

Imaging the Photochemical Ring-Opening of 1,3-Cyclohexadiene by Ultrafast Electron Diffraction

T. J. A. Wolf[1,*], D. M. Sanchez[1,2], J. Yang[1,3], R. M. Parrish[1,2], J. P. F. Nunes[4,5], M. Centurion[5], R. Coffee[3], J. P. Cryan[1], M. Gühr[1,6], K. Hegazy[1,7], A. Kirrander[8], R. K. Li[3], J. Ruddock[9], X. Shen[3], T. Veccione[3], S. P. Weathersby[3], P. M. Weber[9], K. Wilkin[5], H. Yong[9], Q. Zheng[3], X. J. Wang[3,*], M. P. Minitti[3,*], T. J. Martínez[1,2,*]

[1]Stanford PULSE Institute, SLAC National Accelerator Laboratory, Menlo Park, USA.

[2]Department of Chemistry, Stanford University, Stanford, USA.

[3]SLAC National Accelerator Laboratory, Menlo Park, USA.

[4]Department of Chemistry, University of York, Heslington, York, UK.

[5]Department of Physics and Astronomy, University of Nebraska-Lincoln, Lincoln, USA.

[6]Institut für Physik und Astronomie, Universität Potsdam, Potsdam, Germany.

[7]Department of Physics, Stanford University, Stanford, USA.

[8]EaStCHEM, School of Chemistry, University of Edinburgh, Edinburgh EH9 3FJ, United Kingdom.

[9]Department of Chemistry, Brown University, Providence, USA.

Abstract:

The ultrafast photoinduced ring-opening of 1,3-cyclohexadiene constitutes a textbook example of electrocyclic reactions in organic chemistry and a model for photobiological reactions in vitamin D synthesis. Here, we present direct and unambiguous observation of the ring-opening reaction path on

the femtosecond timescale and sub-Ångström length scale by megaelectronvolt ultrafast electron diffraction. We follow the carbon-carbon bond dissociation and the structural opening of the 1,3-cyclohexadiene ring by direct measurement of time-dependent changes in the distribution of interatomic distances. We observe a substantial acceleration of the ring-opening motion after internal conversion to the ground state due to steepening of the electronic potential gradient towards the product minima. The ring-opening motion transforms into rotation of the terminal ethylene groups in the photoproduct 1,3,5-hexatriene on the sub-picosecond timescale. Our work demonstrates the potential of megaelectronvolt ultrafast electron diffraction to elucidate photochemical reaction paths in organic chemistry.

Main text

The photoinduced ring-opening of 1,3-cyclohexadiene (CHD) yielding 1,3,5-hexatriene (HT) is a prototypical electrocyclic reaction that provides a model system for understanding vitamin D generation.[1,2] As with any photoinduced electrocyclic reaction, the ring-opening of CHD is characterized by concerted rearrangement of single and double bonds and strong stereoselectivity. The latter is well-described by the celebrated Woodward-Hoffmann rules.[3] Analogous reactions enable many otherwise difficult transformations in organic synthesis[4] and serve as the basis for many molecular switches.[5]

After photoexcitation at 267 nm to the first excited singlet state (S_1, see Fig. 1), the ring-opening reaction proceeds by nonradiative relaxation through a conical intersection (CI) to the ground state (S_0) of the reaction product HT.[1,6–8] Near the CI, correlated motion of electrons and nuclei leads to efficient nonadiabatic transitions from S_1 to S_0. The energy of the absorbed photon initially alters only the electronic wavefunction, but is rapidly translated into a rearrangement of atoms, *i.e.* a photochemical reaction.

In the case of CHD ring-opening, a ring of four single and two double C-C bonds is transformed into an alternating chain of three double and two single C-C bonds. There are three structural isomers of the ring-opened HT photoproduct (see Fig. 1 and Supplementary Discussion 1), differing by torsions about the C-C single bonds. The barriers separating these isomers are low (≈0.2eV) compared to the excess energy from the absorbed photon that is available to the nuclei after relaxation to S_0 (≈3.8eV).[6] Therefore, the ground state nuclear wavepacket can be expected to evolve into a mixture of all three isomers. Although previous investigations with ps time resolution have shown that ground state equilibration takes place within several to hundreds of ps,[9–11] direct observation of the atomic displacements in both the initial ring-opening and the earliest sub-picosecond ground state isomerization dynamics has yet to be achieved.[1,6]

The ring-opening has been studied extensively in the gas phase by optical and x-ray spectroscopic methods (see Refs.[1,6,12–15] and Refs. cited therein). Due to their preferential sensitivity to changes in the electronic wavefunction, these experiments reveal timescales for population transfer between electronic states through CIs,[16,17] but cannot directly observe structural dynamics on atomic space and time scales. Time-resolved vibrational spectroscopies,[18] which in principle exhibit such sensitivity, are intrinsically insensitive to dynamics along steeply repulsive potentials like the CHD ring-opening path. Pioneering time-resolved x-ray and electron diffraction studies have made impressive progress towards resolving ultrafast structural dynamics of isolated organic molecules,[9,19–23] but until now, have fallen short of either the sub-Å spatial or femtosecond temporal resolution needed to follow photochemical reaction dynamics in these systems. Early influential non-relativistic electron diffraction studies in molecular crystals have provided unambiguous evidence of ultrafast structural dynamics.[24–26] However, the crystalline environment can have a significant influence on the observed dynamics due to constraints on large amplitude motions from crystal packing effects.[27,28]

Recently, seminal megaelectronvolt (MeV) ultrafast electron diffraction (UED) studies of increasing complexity, from rotational dynamics in diatomic N_2[29] to vibrational dynamics in diatomic I_2[30] and dissociative dynamics in penta-atomic CF_3I,[31] demonstrated the resolution in space and time required to elucidate ultrafast structural dynamics outside crystalline environments. In most of these cases, heavy atoms were involved in order to achieve the necessary signal to noise ratio.

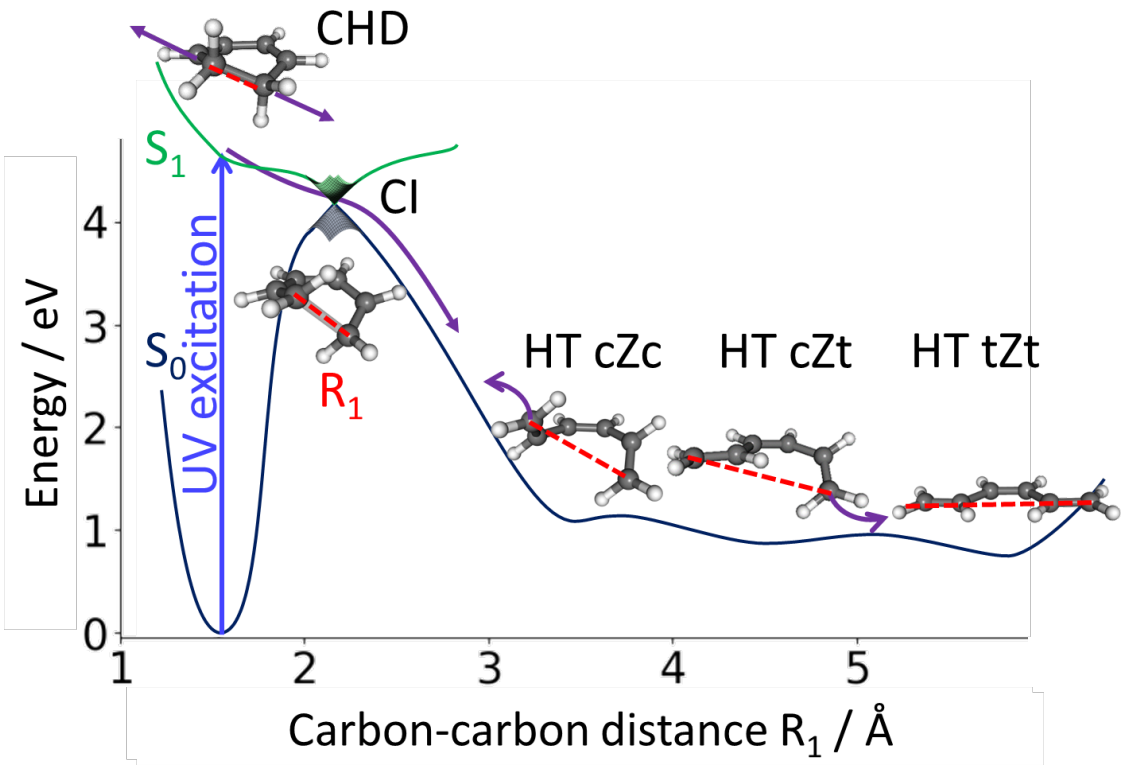

Figure 1: Schematic of the photoinduced ring-opening reaction of 1,3 cyclohexadiene (CHD). CHD is photoexcited from its closed-ring ground state (S_0) energy minimum to an excited state (S_1). It evolves along the ring-opening coordinate (indicated by purple arrows) through a conical intersection (CI) by elongation of the C-C distance R_1 (red) to the S_0 potential energy surface region of 1,3,5-hexatriene (HT). The molecule transforms from a ring containing two conjugated double bonds to a chain of three conjugated ethylene subunits. Twisting about the newly formed single C-C bonds connects three isomers of HT (cZc, cZt, and tZt) via low barriers. The depicted potential energy curves are based on calculated energies at minimum, barrier, and CI geometries (see Supplementary Discussion 2).

In the following, we show that MeV UED allows us to directly observe both the excited state reaction path and subsequent ground state isomerization dynamics for ring-opening in CHD, with sub-Å/femtosecond resolution in space/time for transient changes of atomic distances. Our work resolves atomic motion on femtosecond timescales for the photochemistry of a polyatomic organic molecule containing exclusively light elements with small scattering cross-sections. We believe this is a milestone in enabling MeV UED for general investigations of ultrafast gas phase organic photochemistry. We cover a momentum transfer space (see Fig. 2b and 2d), which is similar to previous ps time-resolved electron diffraction studies[9,19,20,22] but considerably larger than previous fs time-resolved x-ray scattering studies.[21] We approach the maximum momentum transfer range which was recently identified as reasonable for the investigation of structural dynamics in CHD.[32] Therefore, as opposed to the previous x-ray scattering studies, our diffraction data permit reliable transformation into real-space atomic pair distribution functions (PDFs) without any input from theory or simulation. This allows us to directly compare our data to *ab-initio* simulations of the reaction dynamics. As the theory and experiment are completely independent of each other, the successful comparison provides a compelling test of both.

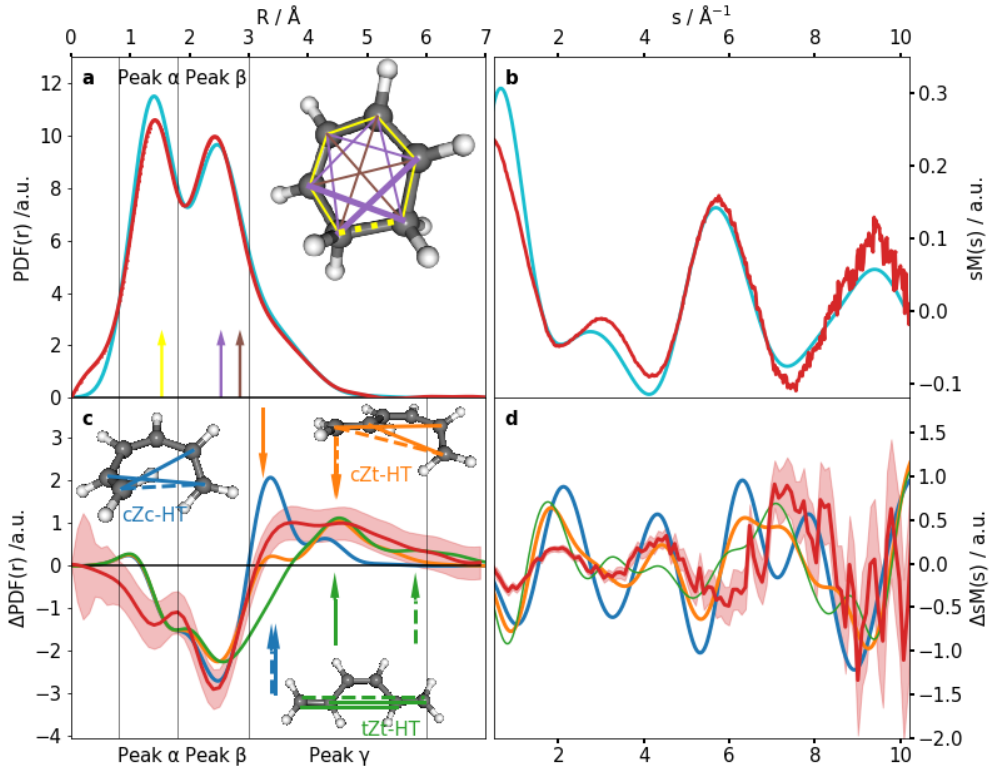

Figure 2: Comparison of experimental and simulated atomic pair distribution functions (PDF). a) Experimental (red) and simulated (light blue) steady-state PDFs of 1,3-cyclohexadiene (CHD) based on an optimized *ab-initio* geometry (see inset and Supplementary Discussion 2-3). The two peaks (α, β, see text) of the PDFs correspond to C-C bond distances (yellow) and C-C distances across the ring (purple, brown). The distances R_1 and R_2, which change significantly during ring-opening, are highlighted by dotted and solid bold lines in the inset. b) Simulated (light blue) and experimental (red) modified molecular diffraction signals, sM(s), for the CHD reactant in momentum-transfer space. c) Steady state simulated difference PDFs (ΔPDFs, PDF_{HT}-PDF_{CHD}) for the three 1,3,5-hexatriene (HT) isomers, cZc-HT (blue), cZt-HT (orange), and tZt-HT (green). For comparison, an experimental ΔPDF at t=0.55 ps is shown (red). The distances R_1 and R_2 (dotted and solid bold lines, respectively) are marked in the geometries and shown as arrows. d) Structural information from c) in momentum-transfer space as difference sM(s) (ΔsM(s)). Error bars represent a 68 % confidence interval obtained from bootstrap analysis.[33]

Results

Figure 2 shows steady-state structural information of CHD in real space (PDF in Fig. 2a) and momentum transfer space (modified molecular diffraction, sM(s), Fig. 2b), respectively. The experimental results are compared with a simple simulation based on an *ab initio*-computed ground state minimum geometry of CHD (see Supplementary Discussion 2 and 3). Experimental and simulated steady-state diffraction signals are in reasonable agreement. The minor observed differences can be ascribed to the method used to subtract the atomic background in the experimental data and the approximation of the ground state nuclear wavefunction by a single geometry (see Supplementary Discussion 3). The corresponding real-space PDFs in Fig. 2a (see Supplementary Discussion 4) exhibit two peaks at 1.4 Å (peak α) and 2.4 Å (peak β). Peak α refers to nearest-neighbor C-C bond distances and peak β is associated with two types of C-C distances across the CHD ring (see inset of Fig. 2a). An additional shoulder at peak β towards larger distances is due to C-H pair correlations. Because the intensity scales with the product of the nuclear charges, the C-H contributions are substantially weaker and H-H contributions are negligible. Accordingly, we will focus on C-C distances below.

The red lines in Figures 2c and 2d respectively show real-space (ΔPDF, see Supplementary Discussion 5) and momentum transfer space (ΔsM) experimental difference signals (time-dependent signature minus static signature) at 0.55 ps time delay, when the ring-opening is complete. They are compared with simulated steady state difference signatures for each of the three HT isomers. We focus our analysis on the real-space representation. In ΔPDFs, the change of an individual C-C distance appears as a pair of correlated features: a negative contribution at the initial value in the CHD reactant and a positive contribution corresponding to its new value at the specific time delay. The ΔPDF is governed by contributions from the C-C distances marked in Fig. 2a and 2c, which undergo substantial changes, whereas contributions to ΔPDF from other distances are weak. The negative signatures coincide with

peaks α and β in the static PDF of CHD and refer to the broken C-C bond (R_1, marked by bold dotted lines in the inset of Fig. 2a) and C-C distances across the ring (R_2, marked by bold solid lines in Fig. 2a), respectively. Moreover, the positive feature (peak γ) between 3 Å and 6 Å, refers to the corresponding C-C distances in HT (see insets of Fig. 2c). Since these distances are larger than those in CHD, the positive peak is direct and unambiguous proof of photoinduced ring-opening.

We compare the experimental ΔPDF in Fig. 2c to simple simulations based on the three isomeric minimum geometries of HT. There is qualitative agreement, with all three ground state isomers and the experimental ΔPDF exhibiting negative signatures below 3 Å and positive signatures beyond 3 Å. However, the experimental ΔPDF clearly does not correspond to a single HT isomer. Furthermore, there is complex structure in the positive signal beyond 3 Å that cannot obviously be attributed to a combination of the equilibrium isomer structures. This is most likely caused by substantial broadening of the nuclear wavepacket due to the large amount of kinetic energy redistributed into nuclear degrees of freedom as the molecule returns to the ground state. We, therefore, refrain from attempts to retrieve transient structures from the experimental data[9,20,24–26] and, instead, interpret them in comparison to explicit wavepacket simulations (see below).

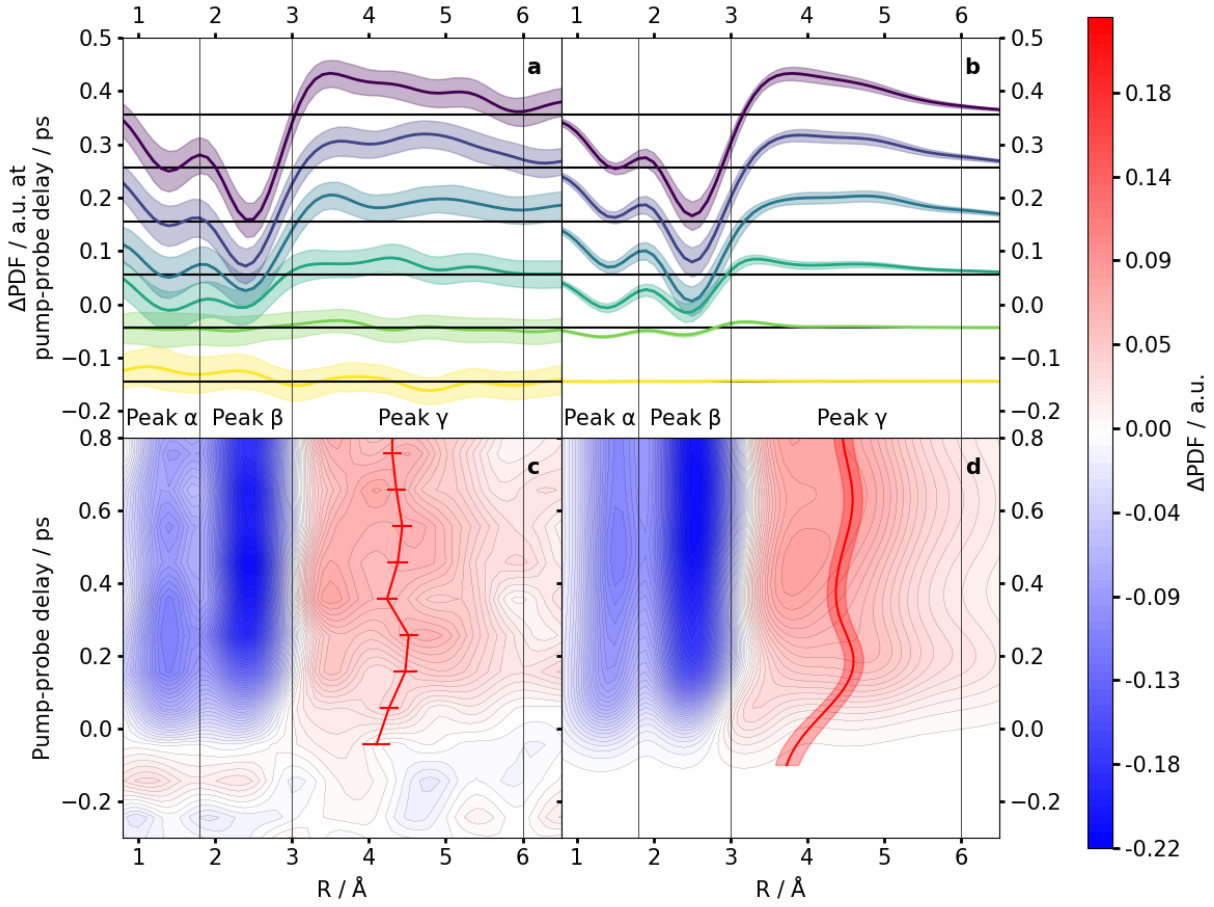

Figure 3: Comparison of experimental (a,c) and simulated (b,d) time-dependent difference pair distribution functions (ΔPDF). a,b) ΔPDFs at different time delays after photoexcitation and c,d) false-color plots of ΔPDF over the whole investigated time window. The plots are separated into peak regions α-γ. The center-of-mass position in peak area γ is shown as red curves in c, d. Simulated ΔPDFs are based on *ab-initio* multiple spawning simulations (see methods) and are convolved with a temporal Gaussian to account for the experimental response function. Error bars represent a 68 % confidence interval obtained from bootstrap analysis.[33] For the simulations, these error bars reflect convergence with respect to initial condition sampling.

Figures 3a and 3c show experimental ΔPDFs at different delay times after photoexcitation (t=0) and a false-color surface plot of the whole dataset. Convolved with the finite instrument response function (160 fs, see Supplementary Discussion 6), they exhibit time-dependent relative intensity changes due to

the underlying structural evolution of the photoexcited molecules. The relative amplitudes of peaks α and β are similar for early delays, but peak β achieves almost twice the amplitude of peak α at later delays (see Fig. 3a). Fitting the changes in relative amplitudes with error functions reveals a delayed rise time (with respect to peak α) for peaks β (70 ± 30 fs) and γ (80 ± 40 fs).

The delayed onset of peaks β and γ directly reflects the ring-opening structural dynamics. During the ring-opening, positive contributions increase in both regions due to lengthening of R_1 and R_2. As shown in Supplementary Figure 1, the delayed rise of peak β can be attributed to the positive contribution from lengthening of R_1 (with amplitude moving from peak α to peak β) compensating for the negative contribution in this region from lengthening of R_2 (with amplitude moving from peak β to peak γ). The delayed rise of peak γ marks the time when R_1 reaches values corresponding to the HT isomers (see Fig. 1) and the ring-opening is complete.

To further elucidate the observed structural changes in the ΔPDFs, we compare our experimental data to *ab-initio* multiple spawning (AIMS) simulations[34] at the α-CASSCF(6,4)/6-31G*[35] level of theory (see methods). The computed ΔPDFs show excellent agreement with experiment (see Fig. 3 and Supplementary Fig. 2). The AIMS simulations also exhibit a delay in the onset of peaks β and γ (Fig. 4) relative to onset of peak α.

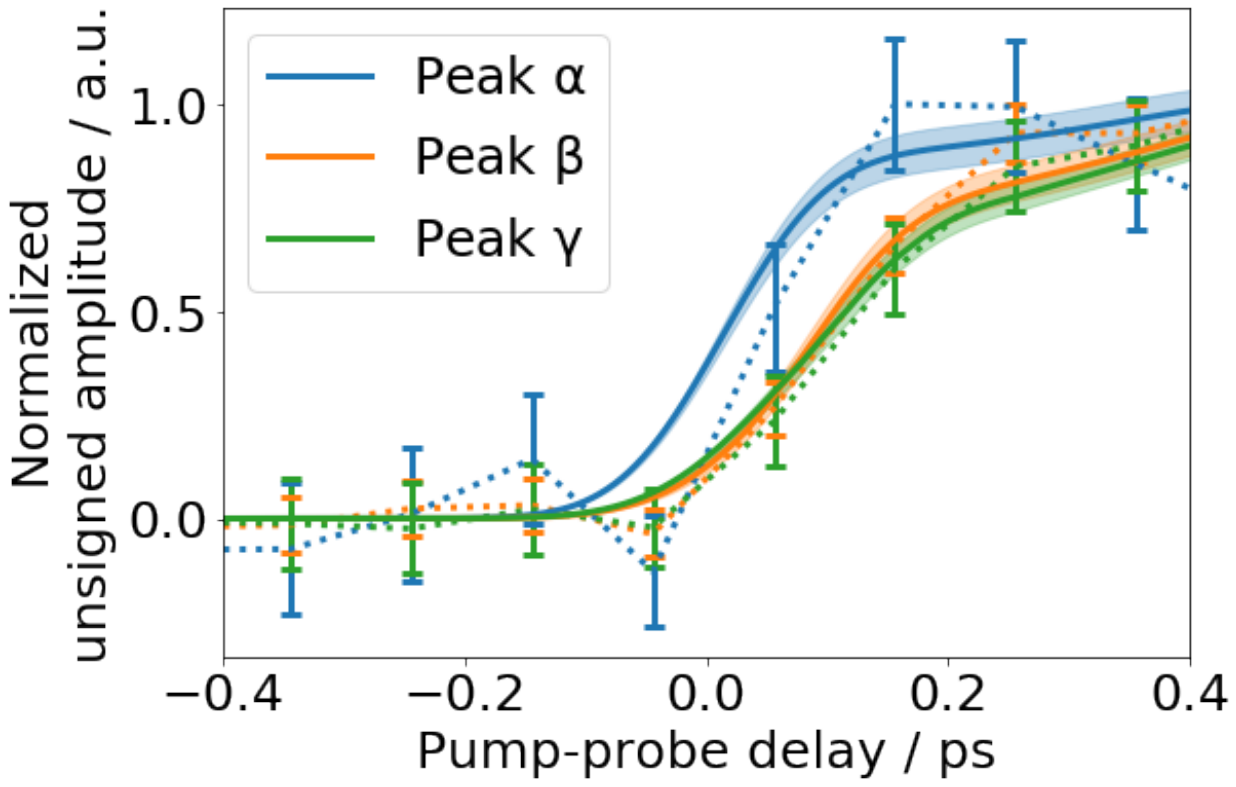

Figure 4: Comparison between experimental and simulated delay in rise time between peaks α, β, and γ. The areas of peak α (0.8 Å – 1.8 Å, blue), peak β (1.8 Å – 3.0 Å, orange), and peak γ (3.0 Å – 6.0 Å, green) in experimental (dotted lines) and simulated (solid lines) ΔPDFs as shown in Fig. 3 are integrated and normalized to the maximum unsigned amplitude. Error bars represent a 68 % confidence interval obtained from bootstrap analysis.[33]

We see breathing-like behavior of peak γ (modulating its width and peak value) in both experimental and simulated ΔPDFs. We quantify this by denoting the time-dependent center-of-mass of peak γ (red curves in Figs. 3c and d), which shows a maximum displacement at 0.25 ps (simulation: 0.2 ps), followed by a minimum at 0.35 ps (0.36 ps), and a weaker second maximum at 0.54 ps (0.59 ps). Comparison with the signatures of the HT isomers in Fig. 2b suggests a coherent oscillation of population between cZc-like and cZt/tZt-like geometries (see Supplementary Discussion 13). Separation of contributions from specific C-C distances in the AIMS dynamics and analysis of the time-dependent isomer distribution (see

Supplementary Figs. 3 and 14-16) indeed proves that the oscillation originates from R_1 and R_2 due to an evolving isomeric composition.

Discussion

As mentioned above, peaks α, β, and γ result from the interplay of positive and negative contributions due to structural changes after photoexcitation. The earliest, negative contribution, peak α, results from the increase in R_1 due to ring-opening. Unlike observables from time-resolved electronic spectroscopy, which usually exhibit features from the quasi-instantaneous response of the molecule's *electrons* to the photoexcitation, the onset of peak α does not mark the time of photoexcitation. Instead, it represents the onset of substantial excited state *nuclear* motion as a response to the photoexcitation, i.e. departure of the molecule from the Franck-Condon region. Thus, some delay is expected between photoexcitation and the onset of peak α. Based on our simulations, this delay is estimated to be 40 fs. Due to relatively small displacements, we are not able to observe other known Franck-Condon active degrees of freedom like the C-C bond alternation (which could be expected to respond more quickly to electronic excitation).

Depletion in the peak β region arises from lengthening of the R_2 distances in the CHD reactant. As discussed above and shown in Supplementary Fig. 1, the delay in the onset of this depletion is due to the simultaneous lengthening of R_1 distances (negative signal in peak α and positive signal in peak β), which partially compensates for the lengthening R_2 distances (negative signal in peak β and positive signal in peak γ). Coincidentally, the R_2 distance in CHD (2.4 Å) is very close to the R_1 distance of the open-minimum energy conical intersection geometry (2.2 Å, S_1/S_0 MECI (Open) in Supplementary Fig. 9) and the R_1 distances where we observe the majority of electronic transitions in the AIMS simulations. Therefore, the rise time of peak β marks the departure of the nuclear wavepacket from the excited state. After accounting for the delay between photoexcitation and the onset of peak α (40 fs), the delay between peak α and peak β (70 ± 30 fs) yields an excited state depopulation timescale of 110 ± 30 fs.

This is in agreement with both excited state lifetimes previously obtained from time-resolved electronic spectroscopy experiments (136 fs, 130 fs, 142 fs, and 139 fs),[13,14,36,37] and AIMS simulations (139 ± 25 fs, see Supplementary Figure 12).

Peak γ corresponds to photoexcited population with R_1 and R_2 distances beyond 2.4 Å. Its rise, thus, exclusively shows structural dynamics on the electronic ground state. This is confirmed by separating excited state and ground state contributions to the simulated ΔPDFs in Supplementary Figs. 4 and 5. Thus, the ring-opening is initiated in the excited state and completed in the ground state, whereas any following isomerization dynamics take place on the ground state. The onset time of peak γ is approximately constant over its whole range between 3 Å and 6 Å. Thus, as opposed to the R_1 increase from 1.4 Å to beyond 2.4 Å resulting in the delay between peaks α and γ, our time resolution is insufficient to fully time-resolve increases in R_1 from 3 Å to 6 Å (see Supplementary Figs. 1, 3, 4, and 5). Hence, the nuclear wavepacket must experience a substantial acceleration upon internal conversion to the ground state. This can be anticipated from the quantum chemical potential sketched in Fig. 1. The conical intersection is only slightly lower in potential energy than the Franck-Condon region. Therefore, the majority of the absorbed photoenergy is released *after* internal conversion to the ground state into the R_1 degree of freedom. In the reaction product HT, this kinetic energy is rapidly converted into twisting motions around the two newly formed single bonds (see Fig. 1) connecting the different HT isomeric minima. The kinetic energy released into the torsional degrees of freedom is so large that the barriers between the HT isomer minima do not play a dominant role. This results in quasi-free rotation of the terminal ethylene groups around the conjugated bonds (see Supplementary Movie 2). The rotation translates to coherent oscillation of the center of mass in peak γ, since the distances probed by this region are a direct reflection of the HT isomers (see Fig. 2 and Supplementary Discussion 13).

Signatures of the rotation of terminal ethylene groups in the HT photoproduct are observed here for the first time. Vacuum ultraviolet and soft x-ray electronic spectroscopic investigations showing signatures of the HT photoproduct do not seem to be sensitive to its isomerization dynamics.[12,13] The product distribution resulting from HT isomerization dynamics has been observed by previous ps UED experiments, but the isomerization mechanism could not be resolved.[9] Other UED studies observed formation of the tZt-HT isomer to take place within 20 ps.[11] In contrast, our study shows both theoretical and experimental evidence that the tZt-HT isomer is already accessed within 0.25 ps after photoexcitation. Signatures of the three HT isomers can be distinguished in solution phase transient absorption spectra.[38] However, in solution environments the solvent is expected to quickly dissipate vibrational excess energy from the solute. The resulting vibrational cooling renders the HT isomerization barrier heights significant enough to prevent terminal ethylene rotation, substantially altering the isomerization dynamics.

In conclusion, by following the femtosecond changes in the atomic distances R_1 and R_2, we demonstrate the first direct observation of the photoinduced structural ring-opening in isolated CHD, a model for the photosynthesis of previtamin D_3. Moreover, we find that the majority of the excess kinetic energy is released after return to the electronic ground state into a specific motion of the HT photoproduct - the quasi-free rotation of the terminal ethylene groups around the conjugated C-C bonds. This results in coherent oscillations in the atomic pair distribution signatures of the HT photoproduct, reflecting a highly non-equilibrium time-dependent oscillatory distribution of HT isomers. Our results showcase the promise of megaelectronvolt ultrafast electron diffraction for the study of ultrafast photochemistry and photobiology.

Methods:

Megaelectronvolt gas phase ultrafast electron diffraction: The gas-phase ultrafast electron diffraction (UED) apparatus is described in detail elsewhere[29,39]. In short, we use the 800 nm output of a Ti:Sapphire laser system operated at 180 Hz repetition rate and separate two beam paths. Pulses in both beam paths are frequency tripled. The pulses of the probe beam path are directed onto the photocathode of an RF gun and eject an ultrashort pulse containing ~10^4 electrons. The electrons are rapidly accelerated in a microwave cavity to a kinetic energy of 3.7 MeV and focused through a holey mirror to a spot size of 200 µm FWHM in the interaction region of a gas phase experimental chamber. The pump pulses (50 µJ) are focused into the experimental chamber to a diameter of 250 µm FWHM and overlapped with the electron pulses at a 5° angle. The experimental response function including effects of the optical and electron pulse length as well as relative arrival time jitter is estimated to be 160 fs (see Supplementary Discussion 6). The sample 1,3-cyclohexadiene (CHD) is purchased from Sigma-Aldrich and used without further purification. We inject CHD vapor with a pulsed nozzle (100 µm orifice) into the interaction region of the experiment. Diffracted electrons are detected by a combination of a phosphor screen and an EMCCD camera. Based on the relative static and dynamic signal levels, we estimate that about 13 % of the molecules are excited (see Supplementary Discussion 7). We additionally perform pump pulse energy scans to confirm that we are in the linear absorption regime (see Supplementary Discussion 8). Time-dependent diffraction is measured at a series of delay time points between -1 and +1.8 ps in each scan. The separation between time delay points is 100 fs, except for the earliest and latest delay points, where it was considerably larger. At each time delay point, we integrate diffraction signal for 20 seconds. The full data set includes 166 such scans. The sequence of delay steps is randomized for every scan to avoid systematic errors. The camera images are azimuthally averaged and calibrated using a value of 0.0224 $Å^{-1}$/pixel based on diffraction of the molecule CF_3I. There is a center hole in the detector for transmitting the undiffracted electrons which cuts the s range at 0.5 $Å^{-1}$. Signal beyond 10.2 $Å^{-1}$ was

not included in analysis due to limited signal-to-noise. The data evaluation is described in detail in Supplementary Discussion 2-5.

Excited state wavepacket dynamics simulations: *Ab-initio* multiple spawning (AIMS) wavepacket simulations[34] interfaced with GPU-accelerated[35,42–45] α-complete active space self-consistent field theory (α-CASSCF) are used to model the photodynamics of isolated CHD. The α-CASSCF method describes static correlation with a multireference CASSCF description of the electronic wavefunction,[40] while mimicking dynamic correlation effects through energy scaling (α).[35,41] Our active space consists of six electrons in four orbitals determined to minimize the average energy of the lowest two singlet states, within the 6-31G* basis set,[46] i.e. α-SA-2-CASSCF(6,4)/6-31G*. Electronic structure calculations are performed with TeraChem.[47–49] Following previous work,[35] we use an α value of 0.82. Electronic structure details and validation tests are given in Supplementary Discussion 9 and 10.

The first two singlet states (S_0 and S_1) are included in the dynamics. All required electronic structure quantities (energies, gradients, and nonadiabatic couplings) are calculated as needed with α-SA-2-CASSCF(6,4)/6-31G*. An adaptive timestep of 0.48 fs (20 au) (reduced to 0.12 fs (5 au) in regions with large nonadiabatic coupling) is used to propagate the centers of the trajectory basis functions (TBFs). A coupling threshold of 0.01 au (scalar product of nonadiabatic coupling and velocity vectors) demarcates spawning events generating new TBFs on different electronic states. Population transfer between TBFs is described by solving the time-dependent Schrödinger equation in the time-evolving TBF basis set. More details on AIMS are provided in Supplementary Discussion 11.

We simulate the first 1 ps of ultrafast dynamics for CHD by: 1) using AIMS to propagate the initial wavepacket for the first 500 fs or until all population has returned to the ground state, 2) stopping TBFs on the ground state when they are decoupled from other TBFs (off-diagonal elements of the Hamiltonian become small), and 3) adiabatically continuing these stopped TBFs using the positions and

momenta from the last frame in AIMS as initial conditions for adiabatic molecular dynamics with unrestricted DFT using the Perdew-Burke-Ernzerof hybrid exchange-correlation functional,[50] i.e uPBE0/6-31G*. A total of 116 TBFs are propagated, with 86 of these being adiabatically continued on the ground state with DFT.

Following previous studies,[9,19–21] the computed time-dependent molecular diffraction from the AIMS/DFT trajectories are generated using the independent atom model (IAM) (see Supplementary Discussion 12). The computed diffraction signal is then processed in the same way as the experimental diffraction signal in order to generate simulated time-dependent PDFs.

Data availability:

The data that support the findings of this study are available from the corresponding authors upon reasonable request.

Code availability:

The code used for analysis of the raw experimental and simulation data, and for generation of the manuscript figures is available from the corresponding authors upon reasonable request.

Author contributions:

T. J. A. Wolf, J. Yang, J. P. F. Nunes, M. Centurion, R. Coffee, J. P. Cryan, M. Gühr, K. Hegazy, R. K. Li, X. Shen, T. Vecchione, S. P. Weathersby, K. Wilkin, Q. Zheng, X. Wang, and M. P. Minitti prepared and conducted the experiment at the SLAC ultrafast electron diffraction facility.

D. M. Sanchez, R. M. Parrish, and T. J. Martinez performed the *ab-initio* simulations.

T. J. A. Wolf analysed the experimental data.

T. J. A. Wolf, D. M. Sanchez, J. Yang, R. M. Parrish, M. Centurion, M. Gühr, A. Kirrander, J. Ruddock, P. M. Weber, H. Yong, X. Wang, M. P. Minitti, and T. J. Martinez interpreted the results.

T. J. A. Wolf, D. M. Sanchez, R. M. Parrish, and T. J. Martinez wrote the manuscript.

All authors discussed the science of the paper.

Author information:

Reprints and permissions information is available at www.nature.com/reprints.

The authors declare no competing financial interests.

Correspondence and requests for materials should be addressed to thomas.wolf@stanford.edu, wangxj@slac.stanford.edu, minitti@slac.stanford.edu, todd.martinez@stanford.edu.;

References:

1. Arruda, B. C. & Sension, R. J. Ultrafast polyene dynamics: the ring opening of 1,3-cyclohexadiene derivatives. *Phys. Chem. Chem. Phys.* **16,** 4439–4455 (2014).
2. Havinga, E. & Schlatmann, J. L. M. A. Remarks on the specificities of the photochemical and thermal transformations in the vitamin D field. *Tetrahedron* **16,** 146–152 (1961).
3. Woodward, R. B. & Hoffmann, R. The Conservation of Orbital Symmetry. *Angew. Chem. Int. Ed.* **8,** 781 (1969).
4. Bach, T. & Hehn, J. P. Photochemical Reactions as Key Steps in Natural Product Synthesis. *Angew. Chem. Int. Ed.* **50,** 1000–1045 (2011).
5. Irie, M. Diarylethenes for Memories and Switches. *Chem. Rev.* **100,** 1685–1716 (2000).
6. Deb, S. & Weber, P. M. The Ultrafast Pathway of Photon-Induced Electrocyclic Ring-Opening Reactions: The Case of 1,3-Cyclohexadiene. *Annu. Rev. Phys. Chem.* **62,** 19–39 (2011).

7. Hofmann, A. & de Vivie-Riedle, R. Quantum dynamics of photoexcited cyclohexadiene introducing reactive coordinates. *J. Chem. Phys.* **112,** 5054–5059 (2000).
8. Celani, P., Ottani, S., Olivucci, M., Bernardi, F. & Robb, M. A. What Happens during the Picosecond Lifetime of 2A1 Cyclohexa-1,3-diene? A CAS-SCF Study of the Cyclohexadiene/Hexatriene Photochemical Interconversion. *J. Am. Chem. Soc.* **116,** 10141–10151 (1994).
9. Ruan, C.-Y. *et al.* Ultrafast diffraction and structural dynamics: The nature of complex molecules far from equilibrium. *Proc. Natl. Acad. Sci.* **98,** 7117–7122 (2001).
10. Pullen, S. H., Anderson, N. A., Walker, L. A. & Sension, R. J. The ultrafast photochemical ring-opening reaction of 1,3-cyclohexadiene in cyclohexane. *J. Chem. Phys.* **108,** 556–563 (1998).
11. Cardoza, J. D., Dudek, R. C., Mawhorter, R. J. & Weber, P. M. Centering of ultrafast time-resolved pump–probe electron diffraction patterns. *Chem. Phys.* **299,** 307–312 (2004).
12. Attar, A. R. *et al.* Femtosecond x-ray spectroscopy of an electrocyclic ring-opening reaction. *Science* **356,** 54–59 (2017).
13. Adachi, S., Sato, M. & Suzuki, T. Direct Observation of Ground-State Product Formation in a 1,3-Cyclohexadiene Ring-Opening Reaction. *J. Phys. Chem. Lett.* **6,** 343–346 (2015).
14. Pemberton, C. C., Zhang, Y., Saita, K., Kirrander, A. & Weber, P. M. From the (1B) Spectroscopic State to the Photochemical Product of the Ultrafast Ring-Opening of 1,3-Cyclohexadiene: A Spectral Observation of the Complete Reaction Path. *J. Phys. Chem. A* **119,** 8832–8845 (2015).
15. Kotur, M., Weinacht, T., Pearson, B. J. & Matsika, S. Closed-loop learning control of isomerization using shaped ultrafast laser pulses in the deep ultraviolet. *J. Chem. Phys.* **130,** 134311 (2009).
16. Wolf, T. J. A. *et al.* Probing ultrafast ππ* / nπ* internal conversion in organic chromophores via K-edge resonant absorption. *Nat. Commun.* **8,** 29 (2017).
17. Stolow, A. & Underwood, J. G. Time-Resolved Photoelectron Spectroscopy of Nonadiabatic Dynamics in Polyatomic Molecules. in *Advances in Chemical Physics* **139,** 497 – 587 (Wiley, 2008).
18. Herbst, J., Heyne, K. & Diller, R. Femtosecond Infrared Spectroscopy of Bacteriorhodopsin Chromophore Isomerization. *Science* **297,** 822–825 (2002).

19. Ihee, H. *et al.* Direct Imaging of Transient Molecular Structures with Ultrafast Diffraction. *Science* **291,** 458–462 (2001).
20. Srinivasan, R., Lobastov, V. A., Ruan, C.-Y. & Zewail, A. H. Ultrafast Electron Diffraction (UED). *Helv. Chim. Acta* **86,** 1761–1799 (2003).
21. Minitti, M. P. *et al.* Imaging Molecular Motion: Femtosecond X-Ray Scattering of an Electrocyclic Chemical Reaction. *Phys. Rev. Lett.* **114,** 255501 (2015).
22. Dudek, R. C. & Weber, P. M. Ultrafast Diffraction Imaging of the Electrocyclic Ring-Opening Reaction of 1,3-Cyclohexadiene. *J. Phys. Chem. A* **105,** 4167–4171 (2001).
23. Küpper, J. *et al.* X-Ray Diffraction from Isolated and Strongly Aligned Gas-Phase Molecules with a Free-Electron Laser. *Phys. Rev. Lett.* **112,** 083002 (2014).
24. Jean-Ruel, H. *et al.* Ring-Closing Reaction in Diarylethene Captured by Femtosecond Electron Crystallography. *J. Phys. Chem. B* **117,** 15894–15902 (2013).
25. Ischenko, A. A., Weber, P. M. & Miller, R. J. D. Capturing Chemistry in Action with Electrons: Realization of Atomically Resolved Reaction Dynamics. *Chem. Rev.* (2017). doi:10.1021/acs.chemrev.6b00770
26. Gao, M. *et al.* Mapping molecular motions leading to charge delocalization with ultrabright electrons. *Nature* **496,** 343–346 (2013).
27. Zimmerman, H. E. & Nesterov, E. E. Development of Experimental and Theoretical Crystal Lattice Organic Photochemistry: The Quantitative Cavity. Mechanistic and Exploratory Organic Photochemistry [1]. *Acc. Chem. Res.* **35,** 77–85 (2002).
28. Zimmerman, H. E. & Zuraw, M. J. Photochemistry in a box. Photochemical reactions of molecules entrapped in crystal lattices: mechanistic and exploratory organic photochemistry. *J. Am. Chem. Soc.* **111,** 7974–7989 (1989).
29. Yang, J. *et al.* Diffractive imaging of a rotational wavepacket in nitrogen molecules with femtosecond megaelectronvolt electron pulses. *Nat. Commun.* **7,** 11232 (2016).

30. Yang, J. *et al.* Diffractive Imaging of Coherent Nuclear Motion in Isolated Molecules. *Phys. Rev. Lett.* **117,** 153002 (2016).
31. Yang, J. *et al.* Imaging CF3I conical intersection and photodissociation dynamics by ultrafast electron diffraction. *Science* accepted (2018).
32. Kirrander, A. & Weber, P. M. Fundamental Limits on Spatial Resolution in Ultrafast X-ray Diffraction. *Appl. Sci.* **7,** 534 (2017).
33. Shao, J. & Tu, D. *The Jackknife and Bootstrap*. (Springer-Verlag, 1995).
34. Ben-Nun, M., Quenneville, J. & Martínez, T. J. Ab Initio Multiple Spawning: Photochemistry from First Principles Quantum Molecular Dynamics. *J. Phys. Chem. A* **104,** 5161–5175 (2000).
35. Snyder, J. W., Parrish, R. M. & Martínez, T. J. α-CASSCF: An Efficient, Empirical Correction for SA-CASSCF To Closely Approximate MS-CASPT2 Potential Energy Surfaces. *J. Phys. Chem. Lett.* **8,** 2432–2437 (2017).
36. Kosma, K., Trushin, S. A., Fuss, W. & Schmid, W. E. Cyclohexadiene ring opening observed with 13 fs resolution: coherent oscillations confirm the reaction path. *Phys. Chem. Chem. Phys.* **11,** 172–181 (2009).
37. Kuthirummal, N., Rudakov, F. M., Evans, C. L. & Weber, P. M. Spectroscopy and femtosecond dynamics of the ring opening reaction of 1,3-cyclohexadiene. *J. Chem. Phys.* **125,** 133307 (2006).
38. Harris, D. A., Orozco, M. B. & Sension, R. J. Solvent Dependent Conformational Relaxation of cis-1,3,5-Hexatriene. *J. Phys. Chem. A* **110,** 9325–9333 (2006).
39. Weathersby, S. P. *et al.* Mega-electron-volt ultrafast electron diffraction at SLAC National Accelerator Laboratory. *Rev. Sci. Instrum.* **86,** 073702 (2015).
40. Roos, B. O. The Complete Active Space Self-Consistent Field Method and Its Applications in Electronic Structure Calculations. *Adv. Chem. Phys.* **69,** 399–445 (1987).
41. Frutos, L., Andruniow, T., Santoro, F., Ferre, N. & Olivucci, M. Tracking the excited-state time evolution of the visual pigment with multiconfigurational quantum chemistry. *Proc. Natl. Acad. Sci. U. S. A.* **104,** 7764 (2007).

42. Hohenstein, E. G., Luehr, N., Ufimtsev, I. S. & Martínez, T. J. An atomic orbital-based formulation of the complete active space self-consistent field method on graphical processing units. *J. Chem. Phys.* **142,** 224103 (2015).
43. Snyder, J. W., Hohenstein, E. G., Luehr, N. & Martínez, T. J. An atomic orbital-based formulation of analytical gradients and nonadiabatic coupling vector elements for the state-averaged complete active space self-consistent field method on graphical processing units. *J. Chem. Phys.* **143,** 154107 (2015).
44. Snyder, J. W., Fales, B. S., Hohenstein, E. G., Levine, B. G. & Martínez, T. J. A direct-compatible formulation of the coupled perturbed complete active space self-consistent field equations on graphical processing units. *J. Chem. Phys.* **146,** 174113 (2017).
45. Snyder, J. W., Curchod, B. F. E. & Martínez, T. J. GPU-Accelerated State-Averaged Complete Active Space Self-Consistent Field Interfaced with Ab Initio Multiple Spawning Unravels the Photodynamics of Provitamin D3. *J. Phys. Chem. Lett.* **7,** 2444–2449 (2016).
46. Hehre, W. J., Ditchfield, R. & Pople, J. A. Self—Consistent Molecular Orbital Methods. XII. Further Extensions of Gaussian—Type Basis Sets for Use in Molecular Orbital Studies of Organic Molecules. *J Chem Phys* **56,** 2257–2261 (1972).
47. Ufimtsev, I. S. & Martínez, T. J. Quantum Chemistry on Graphical Processing Units. 1. Strategies for Two-Electron Integral Evaluation. *J. Chem. Theory Comput.* **4,** 222–231 (2008).
48. Ufimtsev, I. S. & Martinez, T. J. Quantum Chemistry on Graphical Processing Units. 2. Direct Self-Consistent-Field Implementation. *J. Chem. Theory Comput.* **5,** 1004–1015 (2009).
49. Ufimtsev, I. S. & Martinez, T. J. Quantum Chemistry on Graphical Processing Units. 3. Analytical Energy Gradients, Geometry Optimization, and First Principles Molecular Dynamics. *J. Chem. Theory Comput.* **5,** 2619–2628 (2009).
50. Perdew, J. P. Density-functional approximation for the correlation energy of the inhomogeneous electron gas. *Phys Rev B* **33,** 8822–8824 (1986).

Acknowledgements:

This work was supported by the U.S. Department of Energy, Office of Science, Basic Energy Sciences, Chemical Sciences, Geosciences, and Biosciences Division. The experimental part of this research was performed at the SLAC megaelectronvolt ultrafast electron diffraction facility, which is supported in part by the DOE BES SUF Division Accelerator & Detector R&D program, the Linac Coherent Light Source (LCLS) Facility, and SLAC under contract Nos. DE-AC02-05-CH11231 and DE-AC02-76SF00515. M. G. is funded via a Lichtenberg Professorship of the Volkswagen Foundation. D. M. S. is grateful to the NSF for a graduate fellowship. J. P. F. N acknowledges the support by the Wild Overseas Scholars Fund of Department of Chemistry, University of York. K. W. and M. C. are supported by the U.S. Department of Energy Office of Science, Basic Energy Sciences under Award No. DE-SC0014170. PMW is supported by the U.S. Department of Energy, Office of Science, Basic Energy Sciences, under Award No. DE-SC0017995. A. K. is supported by the Carnegie Trust for the Universities of Scotland (grant ref. CRG050414) and an RSE/Scottish Government Sabbatical Research Grant (ref. 58507).